High-affinity binding to the SARS-CoV-2 spike trimer by a nanostructured, trivalent protein-DNA synthetic antibody

Yang Xu,[1,‡] Rong Zheng,[1,‡] Abhay Prasad,[1,‡] Minghui Liu,[1] Zijian Wan,[2] Xiaoyan Zhou,[2] Ryan M. Porter,[2] Matthew Sample,[1] Erik Poppleton,[1,§] Jonah Procyk,[1] Hao Liu,[1] Yize Li,[3] Shaopeng Wang,[4] Hao Yan,[1,*] Petr Sulc,[1,*] Nicholas Stephanopoulos[1,*]

1. School of Molecular Sciences, Center for Molecular Design and Biomimetics, The Biodesign Institute, Arizona State University, Tempe, AZ-85281, USA

2. School of Electrical, Computer and Energy Engineering, Biodesign Center for Biosensors and Bioelectronics, Arizona State University, Tempe, Arizona 85287, United States

3. School of Life Sciences, ASU-Banner Neurodegenerative Disease Research Center, The Biodesign Institute, Arizona State University, Tempe, AZ-85281, USA

4. School of Biological and Health Systems Engineering, Biodesign Center for Biosensors and Bioelectronics, Arizona State University, Tempe, Arizona 85287, United States

‡ These authors contributed equally to this work

§ Current address: Max-Planck-Institute for Medical Research, Heidelberg, DE-69120, Germany

*hao.yan@asu.edu; psulc@asu.edu; nstepha1@asu.edu

Abstract

Multivalency enables nanostructures to bind molecular targets with high affinity. Although antibodies can be generated against a wide range of antigens, their shape and size cannot be tuned to match a given target. DNA nanotechnology provides an attractive approach for designing customized multivalent scaffolds due to the addressability and programmability of the nanostructure shape and size. Here, we design a nanoscale synthetic antibody ("nano-synbody") based on a three-helix bundle DNA nanostructure with one, two, or three identical arms terminating in a mini-binder protein that targets the SARS-CoV-2 spike protein. The nano-synbody was designed to match the valence and distance between the three receptor binding domains (RBDs) in the spike trimer, in order to enhance affinity. The protein-DNA nano-synbody shows tight binding to the wild-type, Delta, and several Omicron variants of the SARS-CoV-2 spike trimer, with affinity increasing as the number of arms increases from one to three. The effectiveness of the nano-synbody was also verified using a pseudovirus neutralization assay, with the three-arm nanostructure inhibiting two Omicron variants against which the structures with only one or two arms are ineffective. The structure of the three-arm nano-synbody bound to the Omicron variant spike trimer was solved by negative-stain transmission electron microscopy reconstruction, and shows the protein-DNA nanostructure with all three arms attached to the RBD domains, confirming the intended trivalent attachment. The ability to tune the size and shape of the nano-synbody, as well as its potential ability to attach two or more different binding ligands, will enable the high-affinity targeting of a range of proteins not possible with traditional antibodies.

Introduction

The ability of molecules or nanostructures to bind a target in a high-affinity, high-specificity manner is a cornerstone of biology and nanotechnology. Multivalency[1], characterized by multiple, preferably spatially-matched interactions between molecular species, is extensively employed in natural biological systems. This powerful strategy has been adapted by scientists to design novel materials with strong and specific binding to targets of interest. DNA nanotechnology—which relies on the programmable self-assembly of oligonucleotides to construct materials of precise shape, size, and functionalization[2,3]—has provided a robust nanoscale design toolkit for synthesizing biocompatible supra-structures capable of multivalent binding to molecules. These DNA-based nano-scaffolds can precisely position other molecular species (such as aptamers, proteins, peptides, small molecules, or carbohydrates), with a resolution spanning length scales ranging from a few nanometers to hundreds of nanometers or more. Examples of multivalent constructs built from oligonucleotides vary in complexity, from simple homo- and hetero-oligomers on a DNA duplex[4–6] to highly complex, stoichiometrically-defined presentation of ligands in 2D and 3D space using DNA origami nanostructures, designed to probe the effect of ligand spacing on biological activity[7,8].

In one seminal example, Johnston, Chaput, and coworkers used a DNA duplex to control the spacing between two low-affinity peptides (K_D in the micromolar range) in order to match the distance between the two binding sites on a target protein[6]. This peptide-DNA structure, which the authors termed a "synbody" (synthetic antibody), achieved a roughly thousandfold enhancement in binding affinity for the target relative to the constituent peptides, yielding a dissociation constant in the low-nanomolar regime. The binding was highly dependent on the distance and relative rotation between the two peptides, which could be tuned by adjusting the number of DNA base pairs separating them. Subsequent work demonstrated that DNA duplexes could scaffold two or more binding groups (including peptides, Fab domains, small molecules, or carbohydrates) to enhance binding through multivalent interactions[9].

While duplex-based methodologies offer advantages over individual binding groups, they possess inherent limitations due to their smaller size. Moreover, if the binding groups do not directly target a key interface of the protein, the DNA duplex alone may be too small to block the protein's activity. Inspired by the size and nanostructured presentation of the binding arms found in antibodies (namely, IgG molecules, **Fig. 1A**), we asked whether a more complex, rigid DNA nano-scaffold could be designed to present multiple proteins in such a way to enhance binding to a target (**Fig. 1B**). A distinguishing feature of DNA nanostructures, in contrast to antibodies, is their flexible and simple design, which allows them to match the size, shape, and valence of the target. Notably, many IgG molecules do not bind to their target in a multivalent fashion; only one of the variable regions binds at any given time (**Fig. 1C**). This monovalent binding can in turn render antibodies susceptible to antigen escape upon target mutation[10]. By contrast, a protein-DNA synthetic antibody can be precisely tuned to match the distance between two or more binding patches on its target, ensuring robust binding even in the face of mutations in any of these patches (**Fig. 1D**).

As a model target for designing nanostructured, multivalent protein-DNA synthetic antibodies, we selected the SARS-CoV-2 spike trimer, due to the wide range of binding proteins and the ready availability of multiple spike variants with different affinity towards those proteins.

Furthermore, the Covid-19 pandemic underscored the need for high-affinity, virus-specific neutralizing species that could bind to multiple variants of SARS-CoV-2 and block their entry into cells. The trimeric structure of the SARS-CoV-2 spike protein presented an ideal target for nanostructured affinity agents designed to match the threefold symmetry of the spike[11]. Over the past two years, a number of DNA nanotechnology-based approaches have been reported with enhanced binding to SARS-CoV-2 through multivalency. These include structures like wireframe cages[12], 2D sheets/nets[13], trimeric linkers[14], or shell-like DNA origami nanostructures[15]. Many of these approaches used DNA aptamers as their affinity agents, due to their ease of incorporation into an oligonucleotide-based nanostructure. However, despite the great promise of aptamers, they still suffer from certain limitations. Aptamer affinity is often lower compared with many antibodies, there is a scarcity of high-quality aptamers against many targets, and the limited variability of the design space (four nucleotide bases) limits the range of possible targets to which aptamers can specifically bind without off-target effects. By contrast, recent examples that employ full-length antibodies for viral binding[16] use DNA origami composed of hundreds of oligonucleotides, which could hamper their scalability or clinical translation.

Here, in contrast to aptamer- and origami-based approaches, we explore the potential of a trivalent DNA nano-scaffold consisting of only a few strands linked to *de novo* designed mini-protein binders. This approach provides the benefits of a spatially-optimized multivalent binder for robust multi-strain targeting of the SARS-CoV-2 virus, and it emphasizes a minimal design for greater scalability and potential clinical translation. To neutralize the ability of the SARS-CoV-2 virus to infect humans, we aim to inhibit the initial phase of viral infection, where the spike protein receptor binding domain (RBD) binds to the human angiotensin-converting enzyme 2 (hACE2)[17,18]. Our design relies on creating a three-helix DNA bundle with three identical arms that can hybridize to a protein-DNA conjugate that can in turn bind to the three RBDs on the spike, **Fig. 1D**. By tuning the dimensions of the protein-DNA assembly (which we term a nanostructured synthetic antibody, or “nano-synbody”) to match that of the spike trimer, it should be possible to observe enhanced affinity over the monovalent protein, even upon mutation of the RBD, as in the Delta or Omicron variants. The nano-synbody reported here is similar in size to an IgG (~15 nm). However, it diverges by featuring three arms, with inter-arm distances engineered specifically for the distance between the three RBD domains (~7 nm). In this analogy, the size- and shape-tunable DNA scaffold emulates the Fc region of an antibody, whereas the proteins at the ends of the arms mimic the Fv regions. Furthermore, the programmability of DNA nanotechnology allows us to create nano-synbodies with an identical core structure, but displaying one, two, or three arms, and thus directly probe the effect of multivalency.

For the RBD-binding agent, we selected a designed mini-protein (termed “LCB1”) reported by the Baker lab[19]. This choice was influenced by several factors: its compact size (7 kDa, composed of three alpha helices), the ease of mutagenesis and recombinant expression of the protein in *E. coli*, the high thermal stability, and its high-affinity binding as a monomer to the wild-type (WT) spike RBD (K_D in the sub-nanomolar range). To construct the nano-synbody, as shown in **Fig. 2**, we conjugated LCB1 to a 14-nt DNA handle, and hybridized it with complementary handles on a DNA nanostructure. Our results demonstrate that the binding affinity for the spike trimer increases with the number of proteins displayed, and that this binding enhancement translates to improved neutralization of a spike-bearing pseudovirus. Crucially, the multivalency afforded by the nanostructure imparts high affinity for several Omicron variants, whereas the mono- or di-valent

nano-synbodies are ineffective. Finally, to further elucidate the nano-synbody interaction with the Omicron spike (B.1.1.529), we employed negative-stain transmission electron microscopy (nsTEM). Our imaging confirmed that all three LCB1 proteins bind to the "up" conformation of the spike protein, validating the expected multivalent binding mode of the protein-DNA nanostructure.

Results

Design and computational simulation of nano-synbody structure. The SARS-CoV-2 spike trimer consists of three identical glycosylated proteins, each of which contains two functional domains, termed S1 and S2[20]. The receptor-binding domain (RBD) located on the S1 domain plays a pivotal role in mediating the interaction between the virus and the ACE2 receptor on host cells. The conformational change of the S1 domain from the "down" to the "up" state is crucial to this process. Notably, the spatial separation between the three RBD domains in the up state is ~7 nm. We surmised that a three-helix bundle (3HB)-based DNA nanostructure with three identical single-stranded arms should be able to hybridize to, and display, three copies of a complementary DNA-LCB1 conjugate with approximately these distances (see **Fig. S1-3** for the sequences and detailed design of the 3HB structure). The lower portion of the 3HB structure, fortified with several crossovers between helices to ensure rigidity, measures ~4 nm in diameter, and we hypothesized that the three double-stranded DNA arms terminating in LCB1 would splay outwards due to electrostatic repulsion. Considering both the linker between the DNA handle and LCB1, we reasoned that the distance between the three LCB1 proteins at the tips of the nano-synbody arms could readily recapitulate the spacing of the RBD domains on the spike trimer.

To validate that the nano-synbody could indeed display the three proteins at the intended distance—without introducing deleterious strain into the DNA scaffold—we employed the coarse-grained model ANM-oxDNA[21] to simulate the protein-DNA nanostructure. This model represents each nucleotide as a single rigid body, with interactions parametrized to reproduce the structural, thermodynamic and mechanical properties of single-stranded and double-stranded DNA. The model has previously been instrumental in studying a wide range of DNA nanodevices, demonstrating good agreement with experimental results where available[22–24].

In the ANM-oxDNA simulation package, the dynamics of proteins are modeled using an anisotropic network model (ANM). Each amino acid is represented as a single bead, with harmonic potentials between the beads parametrized to reproduce the protein's measured B-factors, thereby capturing its inherent flexibility. The ANM-oxDNA model has been previously shown to correctly reproduce structures of protein-DNA hybrid nanostructures, including using asymmetric harmonic potentials to model the chemical linker connecting them[25]. Here we used multiscale modeling, combining both coarse-grained and fully-atomistic simulations, to parameterize the chemical crosslinks between the nucleotides and amino acids used in the experiment, and to computationally derive B-factor data of the spike proteins (see Supporting Information). We have extended our graphical user interface tool oxView[26] to facilitate the design and setup of simulations for protein-DNA hybrid structures. The designed structure was then characterized *in silico* through molecular dynamics simulations to quantify its flexibility and confirm that the positions of all three LCB1 proteins conjugated to the arms of the DNA nanostructure were suitable for binding the RBD domains on the spike trimer.

In particular, we probed whether the nano-synbody could bind to multiple conformations of the spike trimer, namely two RBD domains up and one domain down (**Fig. 3A**) and all three domains up (**Fig. 3C**). In the latter case, the distances are approximately equal at ~6.5-7 nm (**Fig. 3D**), as can be expected from the symmetric presentation of the three domains. However, in the asymmetric two-up-one-down conformation the inter-RBD distances vary from ~3.5 nm for the nearby up and down domains, and 7-8 nm between the distant up and down domain and two up domains (**Fig. 3B**). Analysis of the root mean square fluctuation (RMSF), seen as overlays on the nano-synbody, show that the LCB1 proteins are easily able to bridge both of these scenarios, with the majority of the structure remaining rigid, and only the tips of the arms fluctuating more than 1.82 nm. The nick sites where the three arms meet the three-helix bundle core impart flexibility to the arms, enabling them to adapt to the distances on the spike protein without incurring any strain in the structure relative to the unbound nano-synbody. This flexibility at the tips of the three arms is also largely due to the 15-atom linkers between the DNA 5'-terminus and the attachment site to the protein surface (**Fig. S5A**). As such, the structure achieves a balance between rigidity (to avoid excessive entropic penalties) and sufficient flexibility to accommodate various conformational states of the spike trimer. Based on these results, we anticipated that the hybrid nano-synbody would bind to the spike trimer without incurring a significant entropic penalty due to confining the structure upon binding. Movies showing the fluctuations of the bound and unbound nano-synbody can be found in the online Supplementary Material.

Synthesis and characterization of nano-synbodies with one, two, or three arms. In order to modify LCB1 with a ssDNA handle, we introduced a unique cysteine residue at the N-terminus. The protein was expressed recombinantly in *E. coli*, and conjugated to a 14-nucleotide, amine-modified DNA handle using the hetero-bifunctional linker sulfosuccinimidyl 4-(N-maleimidomethyl)cyclohexane-1-carboxylate (SMCC), **Fig. 2A, S5A**. Following exposure to a 1:1 ratio of purified SMCC-DNA, we observed successful conjugation of the LCB1 mini binder to the oligonucleotide, resulting in LCB-DNA with approximately 90% yield (**Fig. S5B**). The modified protein-DNA conjugate was purified using anion exchange chromatography to remove excess DNA, followed by His-trap affinity chromatography to remove excess LCB1 (**Fig. S5C**). SDS-PAGE analysis confirmed the purity of the DNA-LCB1 conjugate, which showed a single band with slower mobility compared with the unmodified LCB1 protein (**Fig. S6A**). For the details of protein production, purification, and modification with DNA see the Supporting Information, **Section S1**. To evaluate the binding affinity of DNA-LCB1 to the spike protein, we employed surface plasmon resonance (SPR) analysis using wild-type spike immobilized on gold films. We observed a robust interaction between the LCB1 mini binder and DNA-LCB1 with the spike protein, as indicated by a dissociation constant (K_D) value in the sub-nanomolar range. Both the LCB1 protein and the DNA-LCB1 conjugate showed strong binding affinity to the spike protein, with K_D values ranging from 0.1 to 0.2 nM (**Fig. S6C,D**). These results suggest that the conjugation with the 14-nt DNA handle did not significantly perturb the binding ability of LCB1 protein.

In parallel, we prepared the 3HB nano-scaffold with three ssDNA arms from six constituent strands via a thermal annealing protocol (**Fig. 2B**). Combining the DNA-LCB1 conjugate with the 3HB in a 3:1 ratio, and incubating at 37 °C to allow the DNA to hybridize should yield the protein-DNA nano-synbody, which we term "3-arm" (**Fig. 2C**). One key advantage of DNA as a nanoscaffold is that the number of arms on the nano-synbody can be readily tuned, simply by

truncating one or two of the constituent strands. We thus designed two additional nano-synbodies with only one or two complementary handles to DNA-LCB1 (which we term “1-arm” and “2-arm”, respectively) in order to directly compare the effect of mono- and bi-valency of the structure, compared with the tri-valent 3-arm nano-synbody. The 3HB scaffolds with one, two, and three arms could all be assembled readily from the constituent strands, and showed increased retention by native PAGE (**Fig. 4A, B**). Adding DNA-LCB1 to each of these DNA scaffolds resulted in the 1-arm, 2-arm, and 3-arm nano-synbodies; native PAGE confirmed that the addition of DNA-LCB1 shifted each nano-scaffold to a higher retention, and the addition of each additional LCB1 protein shifted the final nano-synbody relative to the samples with fewer arms. All samples assembled in high yield (>95%), without aggregation, and did not require additional purification before use; indeed, the simplicity of our design will aid in scalable production of the desired nano-synbody. The 3-arm nano-synbody was probed by AFM and showed rod-like structures with dimensions approximately 20 x 4 nm, which matches the expected dimensions of the structure (~19 x 4 nm) (**Fig. 4B** and **S6**). Taken together, our results demonstrate that we can generate nano-synbodies with one, two, or three arms, in high yield, using a simple sequential annealing protocol with only six DNA strands and a single DNA-LCB1 conjugate.

Probing nano-synbody binding to the spike protein and the effect of multivalency. To characterize the binding of the nano-synbodies to the SARS-CoV-2 spike protein RBD—and to directly probe the effect of multivalency—we turned to a competitive enzyme-linked immunosorbent assay (ELISA) that mimics blocking the viral interaction with the hACE2 receptor. In this assay, trimeric spike protein was adsorbed in a 96-well plate, and exposed to a mixture of hACE2 and a nano-synbody of varying concentration. The hACE2 and nano-synbody compete for binding to the spike protein RBD, and the greater the affinity of the nano-synbody for the spike trimer, the lower the binding of hACE2. The amount of hACE2 bound to immobilized spike on the surface can be determined by using an anti-hACE2 antibody conjugated with horseradish peroxidase (HRP), which can generate a colorimetric signal upon addition of 3,3',5,5'-tetramethylbenzidine. The percent of inhibition was calculated based on the HRP signal in the presence vs. absence of the nano-synbody; complete (100%) inhibition would correspond to complete suppression of the fluorescent signal because the ACE2 receptor would be blocked from binding to the immobilized spike trimer. In this fashion, we can directly compare the relative blocking efficiency of the 1-arm, 2-arm, and 3-arm nano-synbodies, with three different variants of the spike protein: the wild-type (WT), Delta (B.1.617.2), and Omicron (B.1.1.529).

As shown in **Fig. 4C**, both the 1-arm and 3-arm nano-synbodies displayed a dose-dependent inhibition of hACE2 binding to the WT spike, with EC50 values of 261 pM and 124 pM, respectively. The only modest enhancement (~two-fold) of binding enhancement upon going from one to three arms is not unexpected, given the already high affinity of LCB1 for the WT spike (which it was designed to bind). As a result of the small difference between the 1-arm and 3-arm structures, we did not examine the 2-arm nano-synbody with the WT spike. By contrast, the EC50 values for the binding of 1-arm, 2-arm, and 3-arm nano-synbodies to the Delta spike were 614 pM, 327 pM, and 189 pM, respectively (**Fig. 4D**). Given the reduced affinity of the Delta variant RBD for LCB1[27], the effect of multivalency can be seen more clearly, with enhancements of 1.7-fold (between 3-arm and 2-arm, and between 2-arm and 1-arm) and 3.2-fold (between 3-arm and 1-arm). Assaying nano-synbody binding to the Omicron spike (**Fig. 4E**) we found an EC50 value

of 8.97 nM for 3-arm, whereas 1-arm and 2-arm nano-synbodies did not fully inhibit hACE2 binding to spike for any of the concentrations tested (EC50 > 50 nM). Given the extensive number of mutations in the Omicron spike—which dramatically reduces the efficacy of, for example, therapeutic antibodies raised against the WT spike[28]—this variant demonstrates the power of a multivalent scaffold, like the 3-arm nano-synbody, to efficiently neutralize it.

To further characterize the binding of the nano-synbody to the spike protein, we turned to SPR analysis. We were particularly interested in comparing our structures to monoclonal antibodies (mAbs) used as SARS-CoV-2 therapeutics, and which have been shown to reduce virus loads and alleviate symptoms in clinical trials. To date, over 1,100 monoclonal antibodies against SARS-CoV-2 have been reported in the literature, with more than 20 currently in clinical evaluation[29]. Among these, Regeneron's antibody cocktail REGN-COV2, which consists of two mAbs, REGN10933 and REGN10987, has been granted emergency-use authorization by the Food and Drug Administration (FDA). While clinical antibodies have shown effectiveness in neutralizing SARS-CoV-2, they exhibit reduced binding affinity for the Omicron variant compared to the wild-type spike[30,31].

We utilized a home-built Kretschmann configuration SPR setup, and activated the carboxylated gold surface with N-hydroxysuccinimide (NHS) 1-ethyl-3-(3-dimethylaminopropyl)carbodiimide (EDC) in order to covalently immobilized the spike protein. These surfaces were used to investigate the binding affinity of the 3-arm nano-synbody as well as the REGN10933 mAb (**Fig. 5**). The antibody showed binding to both the WT and Delta spike proteins, with K_D values of 369 and 720 pM, respectively, but no binding to the Omicron spike was observed, even at high antibody concentrations (**Fig. 5B,D,F**). By contrast, the 3-arm nano-synbody maintained strong binding ability to all tested spike proteins, with K_D values of 18, 22, and 68 pM for the WT, Delta, and Omicron spike proteins, respectively (**Fig. 5A,C,E**). Thus, compared with REGN10933, the trivalent nanostructures showed a 20-fold and 33-fold enhancement in affinity for the WT and Delta spike, and the binding affinity decreased only modestly for the Omicron spike protein. These results again highlight the advantages of our trivalent antibody mimic, compared with a traditional mAb, as a result of the multivalent presentation.

Nano-synbody neutralization of pseudovirus infection. Having established that the nano-synbodies can bind with high affinity to the spike protein trimer, we next investigated its ability to neutralize SARS-CoV-2 infection, using a pseudovirus assay (**Fig. 6**). We engineered pseudovirus particles (according to a reported protocol[32]) bearing spike proteins for the following variants: WT, Delta, and three Omicron sub-variants (BA.1, BA.2, and BA.4/5). The pseudovirus contained either a GFP or a luciferase gene, allowing successful infection to be monitored using either fluorescence or bioluminescence, respectively. Pseudovirus infection was probed using a human embryonic kidney (HEK) 293T cell line transfected with hACE2 receptors; for cell line and pseudovirus characterization see **Fig. S8,9**. We first probed virus neutralization using the GFP gene-bearing pseudovirus. Cells were exposed to the pseudovirus (1×10^6 TU/mL functional titer; TU = transduction units) and 10 nM of the 3-arm structure. As seen in **Fig. 6A-C**, in the absence of the nano-synbody, cells exposed to pseudovirus bearing the WT, Delta, or Omicron BA.1 spike showed cells with extensive green fluorescence, indicating successful infection. Cells lacking the

hACE2 receptor did not show any fluorescence (see **Fig. S8D**). By contrast, addition of the 3-arm nano-synbody resulted in virtually no GFP fluorescence for any of the three variants tested, confirming that at this concentration it could almost completely block pseudovirus infectivity.

For a more quantitative and sensitive measurement of pseudovirus neutralization, we turned to a luciferase-based assay, and quantified IC50 values for the nano-synbodies. Given our previous results, we decided to only compare the 1-arm and 3-arm nano-synbodies in this assay, to determine the maximum enhancement that multivalency could provide. Similar to the ELISA results in **Fig. 4**, the nano-synbodies showed the greatest neutralization for the pseudovirus bearing the WT spike, with IC50 values of 5 and 17 pM for the 3-arm and 1-arm structures, respectively (**Fig. 6E**). This roughly 3-fold change due to the multivalency was also the smallest difference for all the variants tested, once again due to the already high affinity of the LCB1 protein for the WT spike. By contrast, the IC50 values for the 3-arm vs. 1-arm nanostructures were 63 vs. 549 pM for the Delta spike pseudovirus (~9-fold enhancement, **Fig. 6F**); 548 pM vs. 17.4 nM for the Omicron BA.1 spike (~30-fold enhancement, **Fig. 6G**); and 1.4 vs. 27 nM for the Omicron BA.2 spike (~20-fold enhancement, **Fig. 6H**). For the Omicron BA.4 spike, only the 3-arm nano-synbody gave a measurable IC50 (1.3 nM); the 1-arm structure never reached full inhibition (IC50 > 50 nM), **Fig. 6I**. Taken together, these results again demonstrate the potent effect of the trivalent nanostructure, with greater enhancement for variants where the affinity of the individual LCB1 proteins decreases.

Structural characterization of 3-arm nano-synbody bound to the Omicron spike trimer. To more directly probe the binding of the 3-arm nano-synbody, we characterized the 3D structure of the structure bound directly to the spike trimer via negative-stain (ns) TEM. We found that the 3-arm structure showed almost complete binding to both the Delta and Omicron spike trimers at a 1:1 stoichiometric ratio, as evidenced by agarose gel electrophoresis (**Fig. S7**). We next analyzed the Omicron spike trimer (B.1.1.529) both before and after binding to the 3-arm nano-synbody, via nsTEM. We determined the structure to ~20 Å resolution by 3D reconstruction via reference-free 2D classification using the Relion3.1 software (see **Section S1** for the details of sample preparation, TEM image acquisition, and 3D reconstruction). The spike protein alone showed a conformation with one RBD in the “up” position, which aligns with previous high-resolution cryo-electron microscopy characterizations (**Fig. 7A,C**)[33,34]. The single RBD in the up conformation was not well resolved due to structural flexibility compared to the rest of spike trimer. Despite the relatively low resolution of our structure, we were able to distinguish the three individual spike proteins comprising the trimer, including the two RBD domains in the “down” position, characteristic of the virus prior to binding the ACE2 receptor.

By contrast, the 2D class averages of the Omicron spike trimer exposed to the 3-arm nano-synbody showed additional density corresponding to the cylindrical nano-synbody (~5 nm in length), connected with three arms to the S1 domains of the spike trimer (**Fig. 7B,D**). Although the spike protein could be reconstructed (similar to **Fig. 7C**), the flexibility of the DNA nanostructure—which could result from the flexible linkages between the 3HB core of the structure and the three duplex arms, and the flexible linker between the ends of the arms and the LCB1 protein—precluded reconstruction of the full nano-synbody bound to the spike protein, although both the structure core and arms are visible in the 2D class averages. We thus applied

a smaller circular mask that included the S1 domain of the spike trimer and the region where three LCB1 proteins were designed to bind with RBD, while excluding the flexible DNA region (as shown in the 2D class images in **Fig. 7D,E**). The 3D reconstruction map was generated using these 2D classes, which allowed the atomic model of the spike protein (PDB 7UHC)[27] to be docked successfully into the map using rigid body fitting in chimeraX. In this 3D reconstructed image, we were able to observe density corresponding to the three RBD domains in the "up" position, bound to three copies of the LCB1 protein (**Fig. 7E**), matching the reported structure of the monomeric LCB1 bound to RBD by cryo-EM[27]. Furthermore, all three RBDs were resolved in the up position, with distances of ~7nm between them (corresponding closely to the simulated model, **Fig. 3B,D**), and three copies of LCB1 could be resolved bound to the RBDs. These results strongly suggest that all three arms of the nano-synbody are competent to engage with the Omicron spike trimer as designed. Future studies at higher resolution using cryo-EM should be able to further explore the structure of the protein-bound DNA scaffold itself.

Discussion

We have demonstrated that a DNA nano-scaffold can be designed to match the geometry and nanoscale spacing of the SARS-CoV-2 spike trimer, and create a synthetic IgG-inspired antibody mimetic by displaying three copies of an RBD-binding mini-protein. We used a combination of rational design (based on the known properties of DNA nanostructures) and a coarse-grained, protein-DNA model to engineer the hybrid nanostructure. This nano-synbody was able to bind the wild-type, Delta, and several Omicron variants of the spike protein, and neutralize pseudovirus infectivity by blocking the RBD interaction with the ACE2 receptor. The modularity and programmability of the DNA scaffold enabled direct comparison of nano-synbodies with one, two, and three arms; the three-arm structures were shown to have the highest binding affinity (and concomitant neutralization potential), with multivalency playing an increasingly important role for variants with mutations that weakened the monovalent LCB1-RBD interaction. For several Omicron variants, only the 3-arm nano-synbody showed any appreciable binding or activity, highlighting the great power of multivalency to "rescue" a compromised binder. Our system is simple, consisting of only six DNA strands and a single protein-DNA conjugate, while retaining the nanoscale spacing of the three protein ligands. As such, it is more complex than a DNA duplex linker, but much simpler than a DNA origami nanostructure, which can consist of ~200 oligonucleotides. This simplicity will, in turn, allow for modified nucleotides to be used in the future, if necessary, to confer stability and/or reduce immunogenicity for *in vivo* applications.

The concept of trimerization to match the spike protein has been employed extensively by nanotechnological approaches to SARS-CoV-2 neutralization. Indeed, both LCB1[27] and a number of other protein binders[35,36] have been trimerized using either linear or branched linkers in order to enhance the binding affinity. These systems also showed enhanced binding due to multivalency, as well as resistance to mutational escape for multiple variants. Although purely protein-based approaches may, at the moment, be more scalable (via large-scale recombinant expression), a hybrid protein-DNA approach has several advantages over these systems for certain applications. First, DNA nano-scaffolds enable matching the size, shape, and valency of a target to a higher degree than a protein-based scaffold. It is relatively straightforward to tune

the size and shape of a DNA nanostructure from tens to hundreds of nanometers, and include arbitrarily many, different binding agents in a highly precise and stoichiometrically-defined fashion. As such, a DNA nanostructure could, in principle, bind to patches away from a key binding interface, which are less likely to mutate, and block protein-protein interactions by dint of the nanostructure bulk. For example, nanobodies that bind to the N-terminal domain (NTD) of the spike protein have been reported[36], and we are currently exploring creating a heterobivalent nano-synbody that positions one of these nanobodies along with LCB1 to enhance binding to a single spike monomer. Ultimately, a DNA nano-scaffold that spans many tens of nanometers could be used to bind to large protein complexes with high precision, and with a specificity not possible with monovalent binding, in a manner that is challenging with non-oligonucleotide scaffolds.

Moreover, our nano-synbody approach can, in principle, easily integrate multiple types of binding groups, e.g. combining aptamers with small proteins (or other molecular species like carbohydrates[37]). It is also quite facile to attach additional functionality to the DNA scaffold, such as imaging agents, drugs, polymers (e.g. to prolong circulation *in vivo* or prevent protein fouling), other proteins (e.g. Fc domains), or oligonucleotide handles for detection methods like rolling chain amplification[38], hairpin chain reaction[39], or polymerase exchange reaction[40]. We also highlight that the modularity of the DNA nano-scaffold should allow for new binders (e.g. “updated” versions of LCB1[27], or nanobodies[41,42], that can more effectively bind to the Omicron spike) to be swapped in, with minimal re-optimization.

Although in this work we focused on SARS-CoV-2 neutralization, a multivalent antibody-like DNA structure could be used for a number of applications beyond blocking protein-protein interactions. Nano-synbodies could be used to manipulate proteins at the single-molecule level, both to probe their biophysical characteristics (especially in conjunction with DNA nano-mechanical devices[43]), or to position them in two- and three-dimensional space using DNA walkers[44] or “printers”[45]. The ability to release the protein—either by strand displacement or DNA photocleavage—could afford reversible antibody mimics, whereby the nano-synbody blocks a protein-protein interaction until activated by a specific trigger. Nano-synbodies against two different targets can be readily linked using additional DNA strands (or branched junctions), which would enable novel bi- or tri-specific antibody mimics. Finally, DNA nanostructures can be generated in a combinatorial fashion, from a library of constituent pieces, which could enable *in vitro* evolution of a high-affinity nanostructure, as opposed to rational design. We thus envision that our approach could be used to discover novel protein-DNA synthetic antibodies in a process akin to SELEX for aptamers[46], with libraries of nanostructure scaffolds, protein binding groups, or both. The use of DNA to build the scaffold would make it facile to introduce barcodes specifying the structure formed. Combined with the ability to quickly and accurately design and simulate protein-DNA nano-scaffolds with ANM-oxDNA [https://github.com/Jonahowns/oxpy_anm], it should be feasible to combine experimental testing of nanostructure libraries with *in silico* evolution and screening of candidate nano-synbodies. Our design pipeline for protein-DNA hybrids introduced here combines a GUI tool with a multiscale fully-atomistic and coarse-grained modeling to characterize the nanostructures. It can be also used to compare different designs and iteratively optimize them for highest affinity of binding to the target. The tools are available as free software at [https://sulcgroup.github.io/oxdna-viewer], with Jupyter notebook examples for running hybrid DNA-protein simulations at [https://github.com/mlsample/ipy_oxDNA].[47]

Acknowledgements: Research reported in this publication was supported by The National Institute of General Medical Sciences of the National Institutes of Health under grant number DP2GM132931 to N.S., grant number 1R01GM145916-01A1 to N.S. and P.S., and grant number R01GM140193 to S.W. The content is solely the responsibility of the authors and does not necessarily represent the official views of the National Institutes of Health. P.S. acknowledges support from National Science Foundation grant DMR 2239518. The authors are grateful to Prof. Fang Li (U. Minnesota) for providing the spike protein variants used.

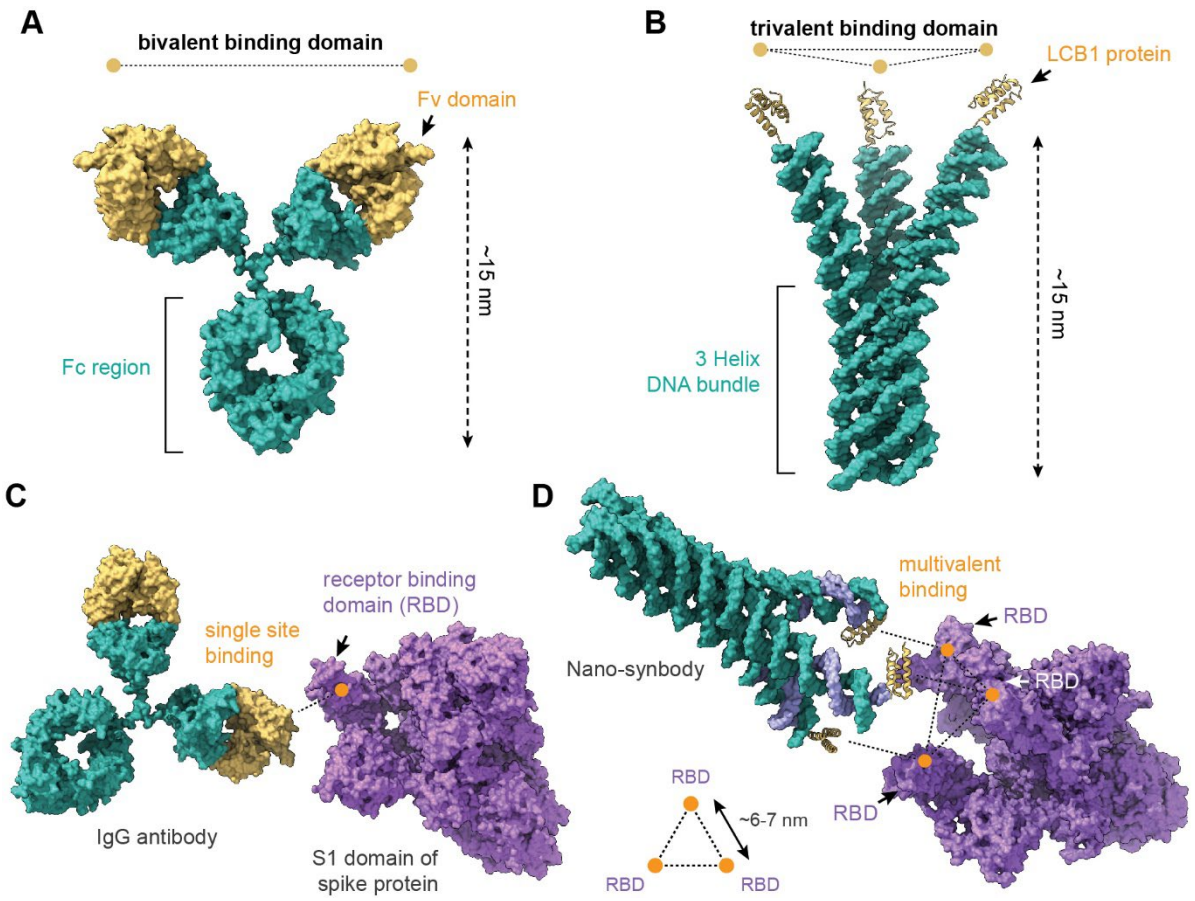

Figure 1. Comparison of an IgG antibody and the protein-DNA nano-synbody. A) Classic Y-shape of an IgG antibody, showing the bivalent presentation of two Fv domains. **B)** Structure of the three-arm nano-synbody, with three LCB1 proteins at the tips of its identical "arms." **C)** Most IgG antibodies can only bind to a target in a monovalent fashion. **D)** The nano-synbody, by contrast, is specifically designed so that the three arms can match the distances between the three binding domains (e.g. the RBD on the SARS-CoV-2 spike trimer).

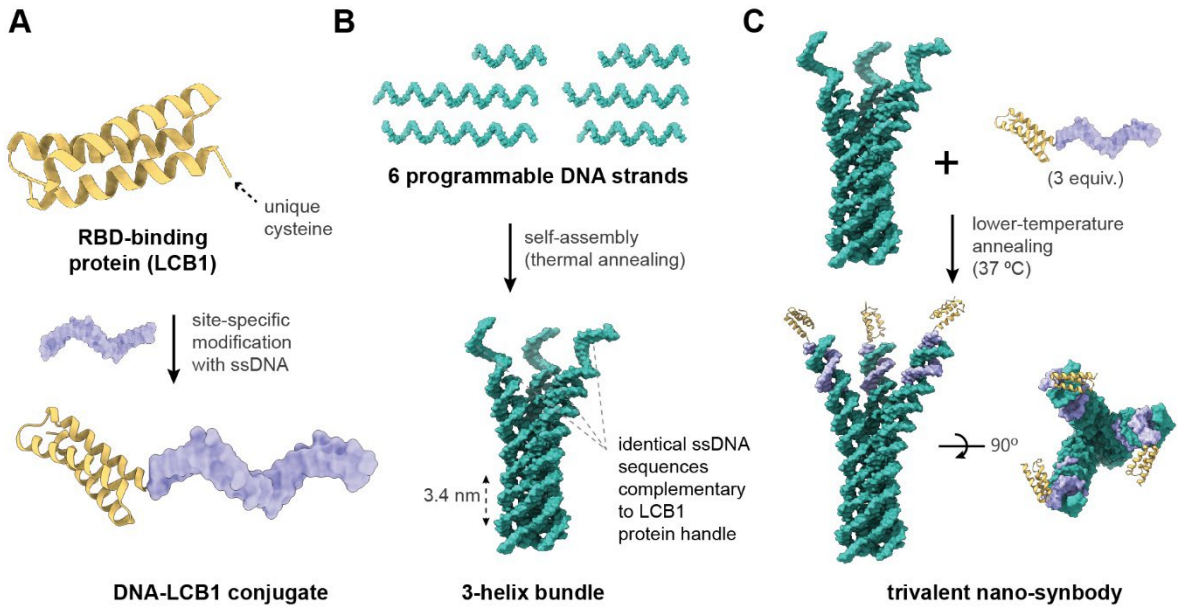

Figure 2. Overview of nano-synbody synthesis. A) The LCB1 mini-binder protein was site-specifically modified with DNA using a unique, mutagenically introduced cysteine residue. **B)** The three-helix bundle (3HB) DNA scaffold was annealed from six unique DNA oligonucleotides. **C)** Incubating the 3HB with the DNA-LCB1 conjugate results in a trivalent nano-synbody.

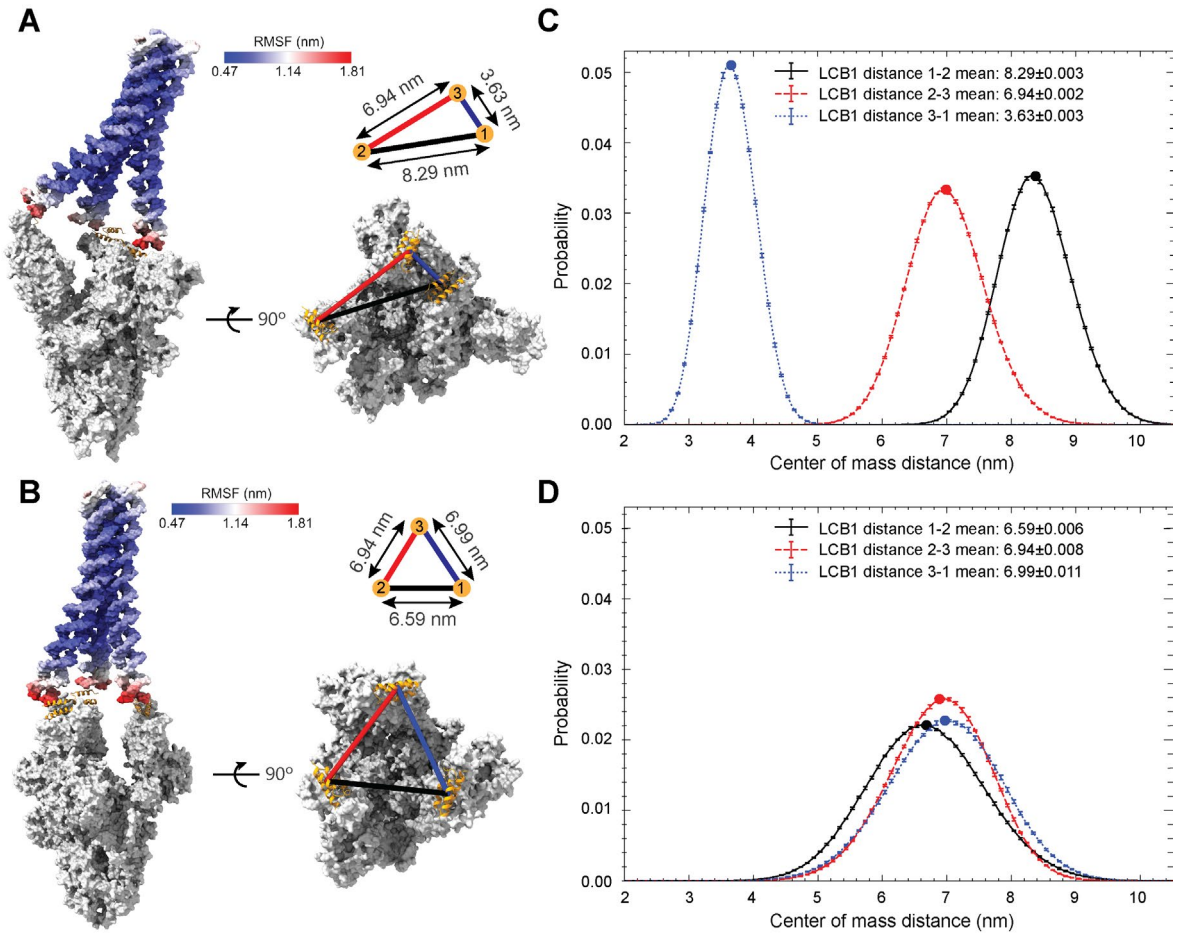

Figure 3. Simulation of three-arm protein-DNA nano-synbody. The nano-synbody, colored according to the root mean-squared fluctuations (RMSF), is depicted bound to the spike protein in two states: with two receptor binding domains (RBDs) up and one down (**A**), and all three RBDs up (**B**). The histograms in (**C**) and (**D**) represent the distance between the center of mass of the LCB1 proteins relative to each other when bound to the spike protein in the two RBD up and three RBD up conformations, respectively. The non-overlapping distributions in (**C**) and overlapping distance distributions in (**D**) quantitatively demonstrate the nano-synbody's capacity to adapt to different distance conditions required to enforce trivalent binding to the spike protein.

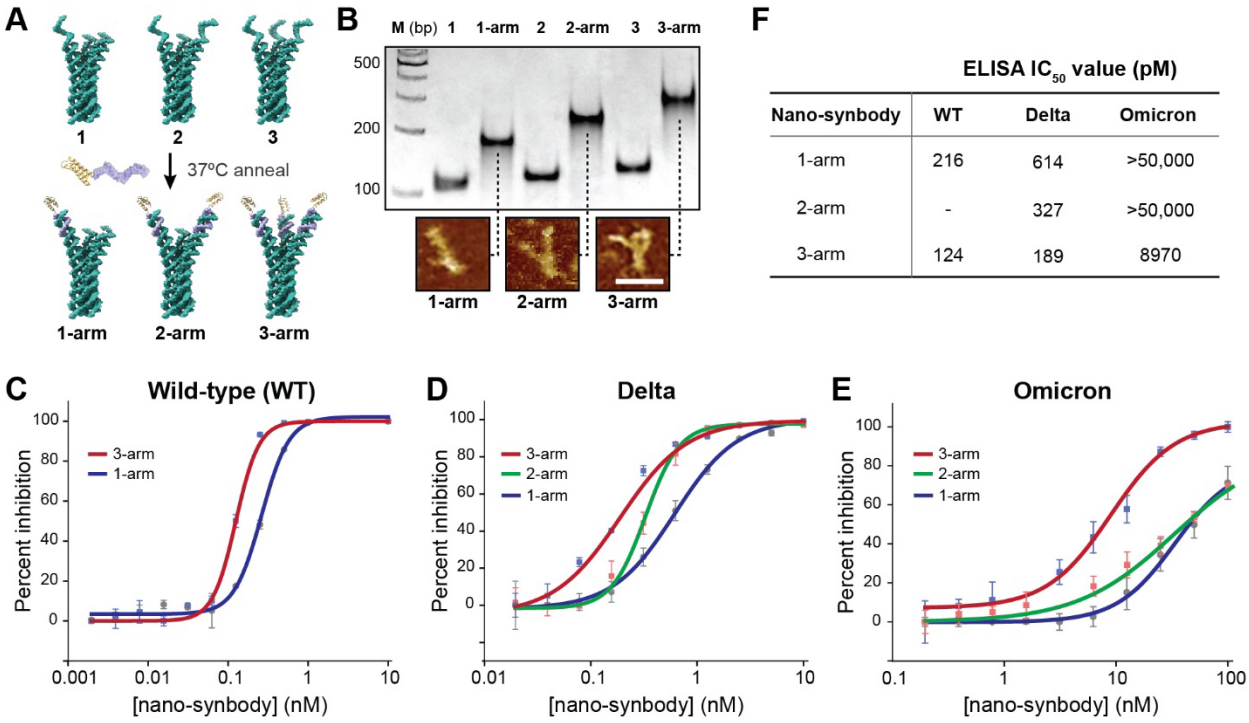

F

	ELISA IC_{50} value (pM)		
Nano-synbody	**WT**	**Delta**	**Omicron**
1-arm	216	614	>50,000
2-arm	-	327	>50,000
3-arm	124	189	8970

Figure 4. Characterization of nano-synbody synthesis and binding by ELISA. A) Three-helix bundles with one (**1**), two (**2**), or three (**3**) ssDNA arms were annealed with equimolar amounts of DNA-LCB1 to yield **1-arm**, **2-arm**, and **3-arm** nano-synbodies. **B)** Native PAGE analysis of the structures from (**A**), showing a shift with increasing arms (lanes **1**, **2**, and **3**) and between samples with and without protein (e.g. **1** vs. **1-arm**, etc.). AFM images show the nano-synbodies with the expected number of arms; to enhance contrast, the samples for AFM were incubated with monomeric RBD prior to imaging. Scale bar: 20 nm. **(C-E)** Competitive ELISA to probe the binding capacity of the nano-synbodies vs. ACE2 for the spike protein. Nano-synbody concentrations were titrated for competition with hACE2-ECD for binding to WT (**C**), Delta (**D**), and Omicron (**E**) spike mutants. Error bars represent the standard deviation (n = 3), and the points were fit with the indicated binding curves. **(F)** Summary of IC50 values for the nano-synbody samples indicated.

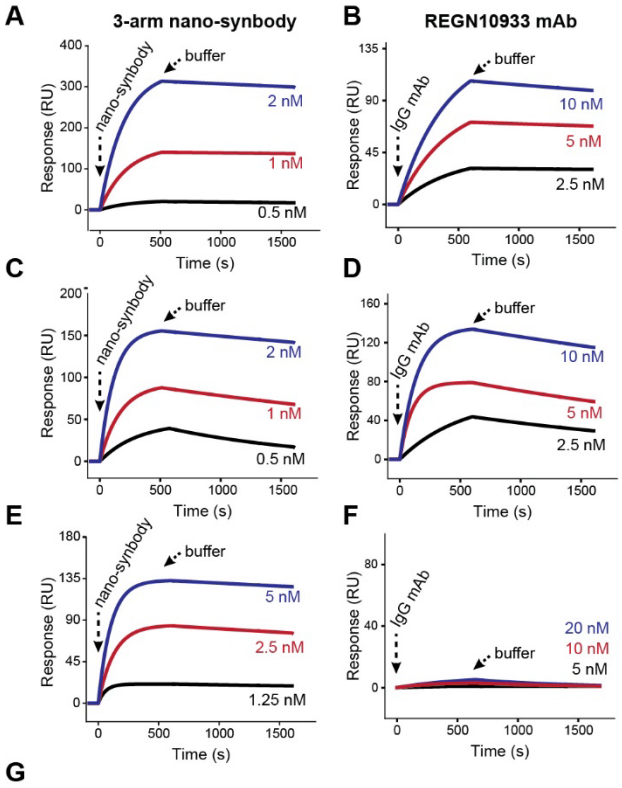

		Wild-type	Delta	Omicron
k_{on} (x 10^5 $M^{-1}s^{-1}$)	3-arm	41.50	41.19	16.0
	IgG mAb	5.59	8.5	N/A
k_{off} (x 10^{-5} s^{-1})	3-arm	4.13	9.67	1.55
	IgG mAb	14.44	59.29	N/A
K_D (x 10^{-12} M)	3-arm	9.96	23.48	97
	IgG mAb	258	690	N/A

Figure 5. Surface plasmon resonance (SPR) characterization of nano-synbody binding. A) SPR sensorgrams depicting 3-arm nano-synbody binding kinetics to the wild-type spike protein. Serial dilutions from 2 to 0.5 nM of SARS-CoV-2 spike protein are represented, and the data were globally fitted with a 1:1 binding model to determine binding affinity. **B)** Sensorgrams illustrating REGN 10933 antibody binding kinetics to the WT spike protein. **(C, D)** Binding kinetics of the Delta spike variant with both the 3-arm nano-synbody (**C**) and the REGN10933 antibody (**D**). **(E, F)** Binding kinetics of Omicron spike with the 3-arm nano-synbody (**E**) and the REGN10933 antibody (**F**). **(G)** Tabulated summary of the kinetic and equilibrium parameters for the studied interactions. "N/A" denotes no observable response at the given concentration.

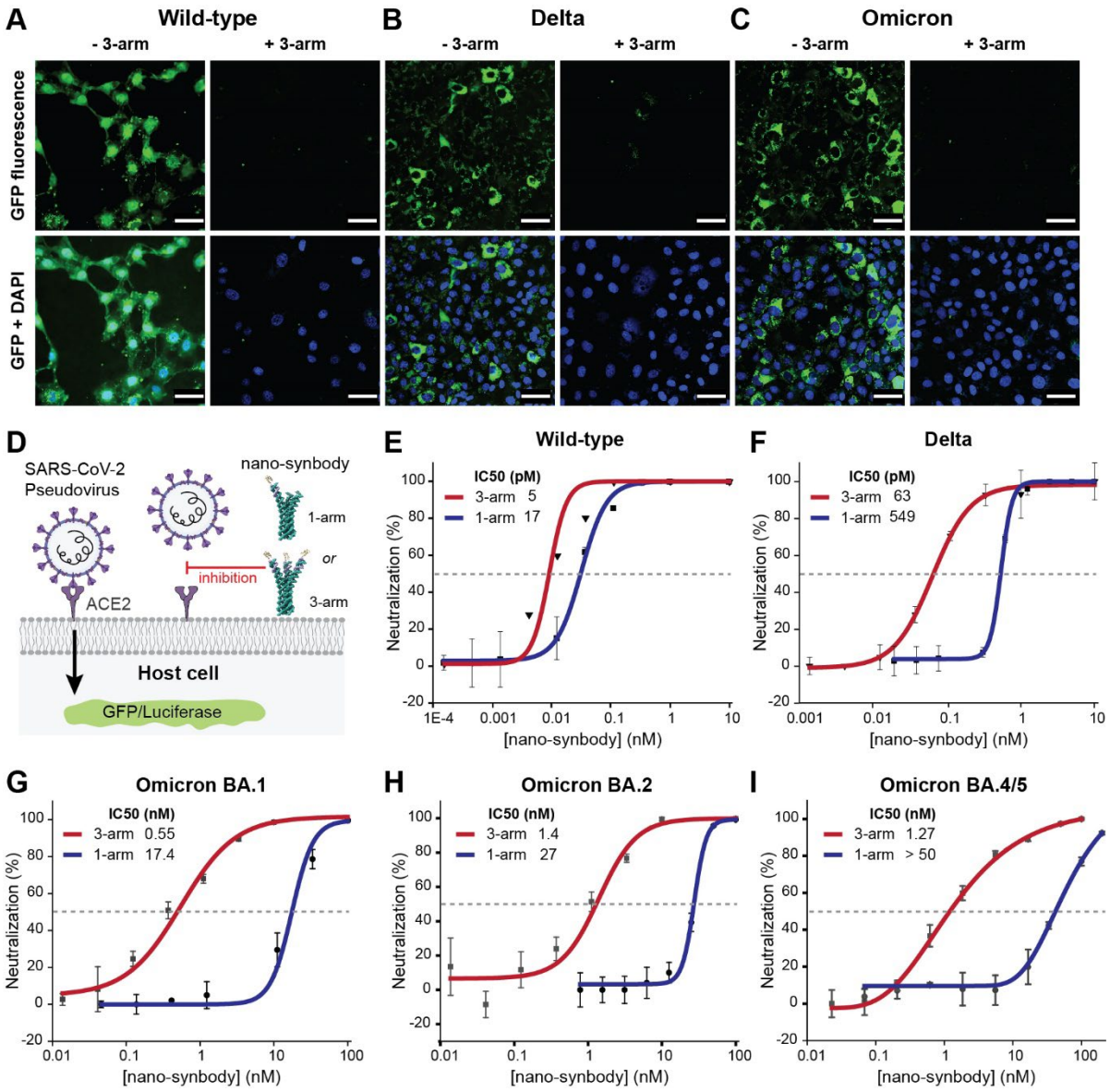

Figure 6. Pseudovirus neutralization assay. A-C) Confocal fluorescence images depicting pseudovirus infection (with GFP cargo) with different spike variants of in the presence or absence of 3-arm nano-synbody (10 nM). Scale bar: 50 μm. **D)** Schematic representation illustrating the neutralization process of SARS-CoV-2 pseudovirus by the nano-synbody. **E-I)** Demonstrated neutralization of the indicated SARS-CoV-2 pseudovirus variants by 3-arm nano-synbody (luciferase cargo). The spike pseudoviruses were subjected to co-incubation with serial dilutions of both 1-arm and 3-arm nano-synbodies for 30 minutes. Subsequently, the mixture was introduced to 293T-ACE2 cells. Following a 36-hour period, the IC50 values for 1-arm or 3-arm nano-synbodies were determined by assessing luciferase expression levels in the 293T-ACE2 cells. Data are representative of three independent experiments. Mean ± SD was shown.

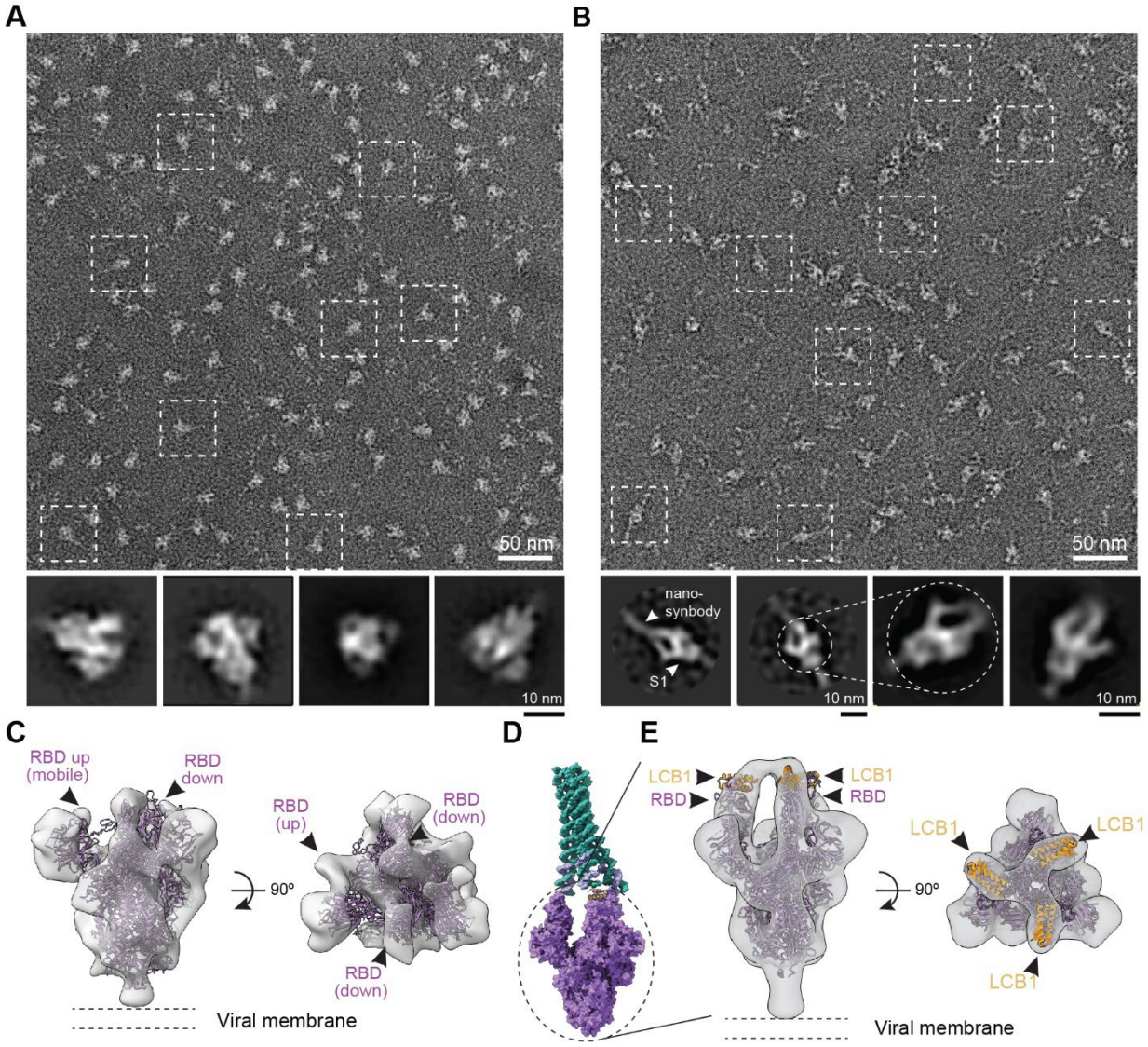

Figure 7. Negative-stain (ns) TEM structural characterization of nano-synbody binding to the Omicron spike trimer. A, B) Representative nsTEM images of the Omicron spike trimer before (**A**) and after (**B**) exposure to the 3-arm nano-synbody. The smaller images show representative 2D class averages for the samples. In (**B**), the 3HB core of the nano-synbody can be distinguished, along with multiple arms binding to the S1 proteins of the spike trimer. **C)** A negative-stain 3D reconstructed EM map (*gray*) of spike trimer in two orthogonal orientations. A cryoEM map (*violet*) of the spike trimer (PDB: 7THK) was docked into the EM map for visualization. **D)** Representative chimera illustration of nano-synbody (*green*) bound with spike trimer (*purple*) with three RBDs in the up conformation. **E)** A focused negative-stain 3D reconstructed EM map of the nano-synbody complex with the spike trimer in two orthogonal conformations. The EM map shows the spike trimer with three RBD in the up conformation and bound to LCB1.

References

1. Fasting, C. *et al.* Multivalency as a chemical organization and action principle. *Angewandte Chemie - International Edition* vol. 51 10472–10498 Preprint at https://doi.org/10.1002/anie.201201114 (2012).
2. Knappe, G. A., Wamhoff, E. C. & Bathe, M. Functionalizing DNA origami to investigate and interact with biological systems. *Nature Reviews Materials* vol. 8 123–138 Preprint at https://doi.org/10.1038/s41578-022-00517-x (2023).
3. Hong, F., Zhang, F., Liu, Y. & Yan, H. DNA Origami: Scaffolds for Creating Higher Order Structures. *Chem Rev* **117**, 12584–12640 (2017).
4. Galimidi, R. P. *et al.* Intra-spike crosslinking overcomes antibody evasion by HIV-1. *Cell* **160**, 433–446 (2015).
5. Bachem, G. *et al.* Rational Design of a DNA-Scaffolded High-Affinity Binder for Langerin. *Angewandte Chemie* **132**, 21202–21208 (2020).
6. Williams, B. A. R. *et al.* Creating protein affinity reagents by combining peptide ligands on synthetic DNA scaffolds. *J Am Chem Soc* **131**, 17233–17241 (2009).
7. Angelin, A. *et al.* Multiscale Origami Structures as Interface for Cells. *Angewandte Chemie - International Edition* **54**, 15813–15817 (2015).
8. Sun, Y. *et al.* DNA origami–based artificial antigen-presenting cells for adoptive T cell therapy. *Sci Adv* **8**, eadd1106 (2022).
9. Freitag, J. S. *et al.* Integration of functional peptides into nucleic acid-based nanostructures. *Nanoscale* vol. 15 7608–7624 Preprint at https://doi.org/10.1039/d2nr05429a (2023).
10. Zhao, Z. *et al.* Omicron SARS-CoV-2 mutations stabilize spike up-RBD conformation and lead to a non-RBM-binding monoclonal antibody escape. *Nat Commun* **13**, 4958 (2022).
11. Koenig, P. A. *et al.* Structure-guided multivalent nanobodies block SARS-CoV-2 infection and suppress mutational escape. *Science (1979)* **371**, eabe6230 (2021).
12. Zhang, J. *et al.* Spatially Patterned Neutralizing Icosahedral DNA Nanocage for Efficient SARS-CoV-2 Blocking. *J Am Chem Soc* **144**, 13146–13153 (2022).
13. Chauhan, N. *et al.* Net-Shaped DNA Nanostructures Designed for Rapid/Sensitive Detection and Potential Inhibition of the SARS-CoV-2 Virus. *J Am Chem Soc* (2022) doi:10.1021/jacs.2c04835.
14. Wan, S. *et al.* Spatial- and Valence-Matched Neutralizing DNA Nanostructure Blocks Wild-Type SARS-CoV-2 and Omicron Variant Infection. *ACS Nano* **16**, 15310–15317 (2022).
15. Monferrer, A. *et al.* DNA origami traps for large viruses. *Cell Rep Phys Sci* **4**, (2023).
16. Sigl, C. *et al.* Programmable icosahedral shell system for virus trapping. *Nat Mater* **20**, 1281–1289 (2021).
17. Benton, D. J. *et al.* Receptor binding and priming of the spike protein of SARS-CoV-2 for membrane fusion. *Nature* **588**, 327–330 (2020).
18. Gong, Y., Qin, S., Dai, L. & Tian, Z. The glycosylation in SARS-CoV-2 and its receptor ACE2. *Signal Transduction and Targeted Therapy* vol. 6 Preprint at https://doi.org/10.1038/s41392-021-00809-8 (2021).

19. Cao, L. *et al.* De novo design of picomolar SARS-CoV-2 miniprotein inhibitors. *Science (1979)* **370**, 426–431 (2020).
20. Walls, A. C. *et al.* Structure, Function, and Antigenicity of the SARS-CoV-2 Spike Glycoprotein. *Cell* **181**, 281-292.e6 (2020).
21. Procyk, J., Poppleton, E. & Šulc, P. Coarse-grained nucleic acid-protein model for hybrid nanotechnology. *Soft Matter* **17**, 3586–3593 (2021).
22. Snodin, B. E. K. *et al.* Introducing improved structural properties and salt dependence into a coarse-grained model of DNA. *Journal of Chemical Physics* **142**, (2015).
23. Doye, J. P. K. *et al.* Coarse-graining DNA for simulations of DNA nanotechnology. *Physical Chemistry Chemical Physics* vol. 15 20395–20414 Preprint at https://doi.org/10.1039/c3cp53545b (2013).
24. Poppleton, E. *et al.* oxDNA: coarse-grained simulations of nucleic acids made simple. *J Open Source Softw* **8**, 4693 (2023).
25. Narayanan, R. P. *et al.* Coarse-Grained Simulations for the Characterization and Optimization of Hybrid Protein-DNA Nanostructures. *ACS Nano* **16**, 14086–14096 (2022).
26. Bohlin, J. *et al.* Design and simulation of DNA, RNA and hybrid protein–nucleic acid nanostructures with oxView. *Nat Protoc* **17**, 1762–1788 (2022).
27. Hunt, A. C. *et al.* Multivalent designed proteins neutralize SARS-CoV-2 variants of concern and confer protection against infection in mice. *Sci Transl Med* **14**, (2022).
28. Tuekprakhon, A. *et al.* Antibody escape of SARS-CoV-2 Omicron BA.4 and BA.5 from vaccine and BA.1 serum. *Cell* **185**, 2422-2433.e13 (2022).
29. Yang, L. *et al.* COVID-19 antibody therapeutics tracker: A global online database of antibody therapeutics for the prevention and treatment of COVID-19. *Antibody Therapeutics* vol. 3 205–212 Preprint at https://doi.org/10.1093/ABT/TBAA020 (2020).
30. Wang, P. *et al.* Antibody resistance of SARS-CoV-2 variants B.1.351 and B.1.1.7. *Nature* **593**, 130–135 (2021).
31. VanBlargan, L. A. *et al.* An infectious SARS-CoV-2 B.1.1.529 Omicron virus escapes neutralization by therapeutic monoclonal antibodies. *Nat Med* **28**, 490–495 (2022).
32. Nie, J. *et al.* Quantification of SARS-CoV-2 neutralizing antibody by a pseudotyped virus-based assay. *Nat Protoc* **15**, 3699–3715 (2020).
33. Cerutti, G. *et al.* Cryo-EM structure of the SARS-CoV-2 Omicron spike. *Cell Rep* **38**, 1214 (2022).
34. Mannar, D. *et al.* SARS-CoV-2 Omicron variant: Antibody evasion and cryo-EM structure of spike protein–ACE2 complex. *Science (1979)* **375**, 760–764 (2022).
35. Hanke, L. *et al.* A bispecific monomeric nanobody induces spike trimer dimers and neutralizes SARS-CoV-2 in vivo. *Nat Commun* **13**, (2022).
36. Schoof, M. *et al.* An ultrapotent synthetic nanobody neutralizes SARS-CoV-2 by stabilizing inactive Spike. *Science (1979)* **370**, 1473–1479 (2020).
37. Kim, S. H. *et al.* SARS-CoV-2 evolved variants optimize binding to cellular glycocalyx. *Cell Rep Phys Sci* **4**, (2023).
38. Xu, M. *et al.* DNA Origami Nanostructures with Scaffolds Obtained from Rolling Circle Amplification. *ACS Mater Lett* **2**, 1322–1327 (2020).
39. Choi, H. M. T., Beck, V. A. & Pierce, N. A. Next-generation in situ hybridization chain reaction: Higher gain, lower cost, greater durability. *ACS Nano* **8**, 4284–4294 (2014).

40. Kishi, J. Y., Schaus, T. E., Gopalkrishnan, N., Xuan, F. & Yin, P. Programmable autonomous synthesis of single-stranded DNA. *Nat Chem* **10**, 155–164 (2018).
41. Chi, X. *et al.* An ultrapotent RBD-targeted biparatopic nanobody neutralizes broad SARS-CoV-2 variants. *Signal Transduct Target Ther* **7**, 44 (2022).
42. Hanke, L. *et al.* An alpaca nanobody neutralizes SARS-CoV-2 by blocking receptor interaction. *Nat Commun* **11**, 4420 (2020).
43. Funke, J. J. & Dietz, H. Placing molecules with Bohr radius resolution using DNA origami. *Nat Nanotechnol* **11**, 47–52 (2016).
44. Song, L., Zhuge, Y., Zuo, X., Li, M. & Wang, F. DNA Walkers for Biosensing Development. *Advanced Science* vol. 9 18 Preprint at https://doi.org/10.1002/advs.202200327 (2022).
45. Benson, E., Marzo, R. C., Bath, J. & Turberfield, A. J. A DNA molecular printer capable of programmable positioning and patterning in two dimensions. *Sci Robot* **7**, (2022).
46. Wilson, D. S. & Szostak, J. W. In vitro selection of functional nucleic acids. *Annual Review of Biochemistry* vol. 68 611–647 Preprint at https://doi.org/10.1146/annurev.biochem.68.1.611 (1999).
47. Sample, M., Matthies, M. & Šulc, P. Hairygami: Analysis of DNA Nanostructure's Conformational Change Driven by Functionalizable Overhangs. arXiv preprint arXiv:2302.09109 (2023).